UC Berkeley
UC Berkeley Previously Published Works

Title

Characterization of a Block Copolymer with a Wide Distribution of Grain Sizes

Permalink

https://escholarship.org/uc/item/7m177121

Journal

ISSN

Authors

Wang, Xin
Chintapalli, Mahati
Newstein, Maurice C
et al.

Publication Date

DOI

Peer reviewed

Characterization of a Block Copolymer with a Wide Distribution of Grain Sizes

Xin Wang,[†] Mahati Chintapalli,[§,⊥] Maurice C. Newstein,[‡] Nitash P. Balsara,[∥,⊥,#] and Bruce A. Garetz[*,†]

[†]Department of Chemical and Biomolecular Engineering and [‡]Department of Electrical and Computer Engineering, NYU Tandon School of Engineering, Brooklyn, New York 11201, United States

[§]Department of Materials Science and Engineering and [∥]Department of Chemical and Biomolecular Engineering, University of California, Berkeley, Berkeley, California 94720, United States

[⊥]Environmental Energy Technologies Division and [#]Materials Sciences Division, Lawrence Berkeley National Laboratory, Berkeley, California 94720, United States

DPLS Detectable Grains   Region occupied by undetectable grains
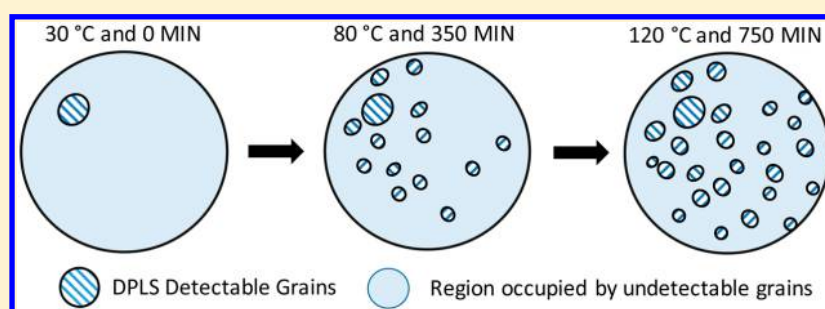
ABSTRACT: Block copolymer/lithium salt mixtures are an emerging class of lithium battery electrolytes. Previous studies have shown that the ionic conductivity of these materials is a sensitive function of grain size. Both depolarized light scattering (DPLS) and small-angle X-ray scattering (SAXS) have proven to be effective techniques for elucidating the grain structure of block copolymer (BCP) materials. DPLS is particularly useful for the characterization of samples with grain sizes larger than 1 μm, whereas SAXS is particularly well suited for samples with grain sizes smaller than 0.1 μm. We present the results of both DPLS and SAXS measurements of grain structure in a BCP/lithium salt mixture that was annealed after being initially prepared by freeze-drying from solution. The combination of the two techniques demonstrates that our sample is characterized by an extremely wide distribution of grain sizes. In particular, the sample has a large population of small sub-micrometer-sized grains that cannot be detected optically. A bimodal grain distribution model is presented to support this interpretation of the experimental data. The presence of both large grains and regions of undetectable small grains was confirmed by polarized optical microscopy (POM). Two-wavelength DPLS measurements provide an additional approach for characterizing block copolymer samples with a broad distribution of grain sizes.

INTRODUCTION

Mixtures of block copolymers (BCPs) and lithium salts are important candidates for lithium battery electrolytes, owing to their combination of rigidity and ionic conductivity.[1−9] These materials undergo a nanoscale phase separation forming lamellae, cylinders, and other morphologies when cooled below the order-to-disorder transition (ODT) temperature, T_{ODT}.[10−15] Coherent order of the lamellae or cylinders is limited to small regions called grains. A recent study has demonstrated that the Li$^+$ ion conductivity of BCP/Li$^+$ salt mixtures is inversely related to grain size.[16]

Over the past 20 years, depolarized light scattering (DPLS) has proven to be extremely useful in characterizing the grain structure of lamellar and cylindrical block copolymers.[14,17−19] The angular spread of the DPLS pattern is inversely related to the average grain size. In particular, average grain sizes, shapes and volume fractions, as well as growth kinetics, can be determined by the analysis of the scattering patterns. Until now, all studies of block copolymer grain structure by DPLS have

involved BCPs with experimentally accessible ODT temperatures, so those samples could be first disordered by heating, followed by ordering upon cooling the sample below the T_{ODT}. The ordered phase initially forms by a process of nucleation and growth, eventually filling the entire sample with grains exhibiting a narrow distribution of sizes.[13,17−23] Further growth of grains is possible through defect annihilation.[15−17,23−28] In all these studies, the resulting grain sizes were on the order of 1−50 μm.[14,17,18,25]

Small-angle X-ray scattering (SAXS) has also been applied to the measurement of grain size in BCPs.[16,26−29] A plot of SAXS intensity vs the scattering vector, q, from an ordered BCP sample exhibits a series of peaks associated with diffraction from the lamellar or cylinder morphology. The position of the primary peak, $q*$, is inversely related to the lamellar or cylinder
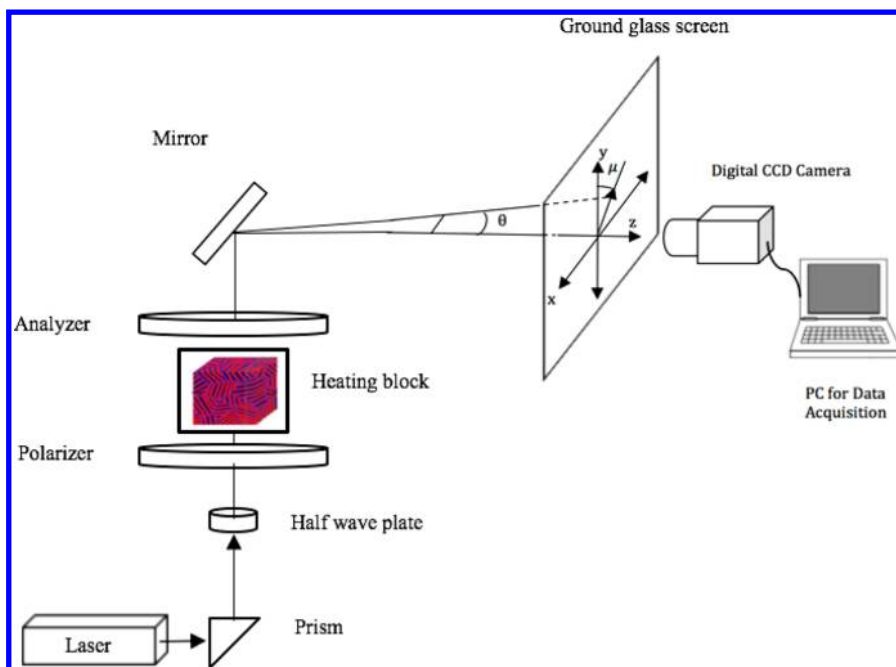
Figure 1. Schematic of depolarized light scattering apparatus and scattering geometry. A scattered light ray deflected from the forward direction is characterized by the angles θ and μ.

domain spacing, while the full width at half-maximum of the primary peak is inversely related to the average grain size.[16,30,31]

Using both DPLS and SAXS, we have analyzed a BCP/lithium salt mixture with an inaccessible ODT. Although the neat polymer had an accessible ODT, the salt concentration of the mixture was sufficiently high that the sample exhibited no ODT in the accessible temperature window and thus could never be disordered. When these samples were made by freeze-drying from solution, they were completely ordered, albeit with a very high defect density (or equivalently, small grain size). Grain structure could be altered irreversibly by annealing the sample at a temperature where grain growth by defect annihilation could occur at a measurable rate. Complete characterization of the grain structure and grain evolution in this sample required a combination of both techniques. A simple model for analyzing the experimental data is presented.

■ EXPERIMENTAL SECTION

Materials. A polystyrene-*block*-poly(ethylene oxide) copolymer (SEO) was synthesized by living anionic polymerization and characterized by methods described in previous publications.[16,32−34] In order to compare the results of SAXS and DPLS measurements, an electrolyte mixture identical to the one used in the SAXS study described in ref 16 was selected for the DPLS measurements described in this paper. The electrolyte mixture was prepared by blending the neat block copolymer, SEO (4.9−5.5), with lithium bis(trifluoromethanesulfonyl)imide (LiTFSI), where the values of 4.9 and 5.5 stand for the molecular weights of individual blocks, which were 4.9 kg mol^{-1} for PS and 5.5 kg mol^{-1} for PEO. The polymer had a polydispersity of 1.04. Prior to mixing, the materials were dried under vacuum; SEO was dried for 24 h at 90 °C, and LiTFSI was dried for 72 h at 120 °C. Salt-containing materials were handled in an argon glovebox with moisture and O_2 levels below 1 ppm. The electrolyte mixture was prepared by dissolving SEO in benzene and adding a concentrated solution of LiTFSI in tetrahydrofuran. The volume of the tetrahydrofuran added to the benzene solution was below 5 vol % to facilitate freeze-drying. The solution was freeze-dried without exposure to air for 1 week. The concentration of the salt (LiTFSI) is represented by an *r*-value, which is the molar ratio of salt molecules to

ethylene oxide groups. In both SAXS and DPLS measurements, the mixture had a concentration of r = 0.085, not far from the concentration of 0.21 that gives the optimal ionic conductivity in homopolymer PEO/LiTFSI mixtures.[35] The mixture does not exhibit an ODT temperature.

The glass transition temperature of the PS phase in SEO (4.9−5.5) with r = 0.085 is ∼71 °C, 7 °C lower than the glass transition temperature of the PS homopolymer of similar molecular weight.[36] The glass transition temperature of the PEO-rich phase is −40 °C, 24 °C lower than the glass transition temperature of the PEO homopolymer.[16,36] The electrolyte mixture has a lamellar microstructure both before and after annealing as determined by SAXS.[32,36,37] Since this fully ordered electrolyte mixture has a degree of microphase separation within the weak segregation regime, the extent of mixing of PS segments in the PEO-rich microphase is considerable; the mobilities of PS and PEO chains are mutually influenced, and they are both strongly dependent on temperature.[36]

Sample Preparation. The samples for DPLS were prepared by pressing freeze-dried electrolyte into a spacer at room temperature. Exposure to heat during sample preparation was avoided to prevent irreversible grain growth before DPLS and SAXS measurements.[25] The dry electrolyte mixture filled a 0.793 mm thick polytetrafluoroethylene spacer with an inner diameter of 4.76 mm. The sample was sandwiched between two quartz windows in a custom-made air-free aluminum sample holder. This sandwiched sample was vacuum-sealed in an aluminum-reinforced polypropylene pouch in an argon glovebox. The steps described above were conducted at Berkeley. The pouched samples were shipped to Brooklyn for the light scattering and polarized optical microscopy (POM) studies.

The samples for SAXS were prepared using a similar procedure, which is described in detail in ref 16. Briefly, freeze-dried electrolyte was pressed at room temperature into a fiberglass spacer (Garolite G10), 0.150 mm thick, with a 3.175 mm inner diameter. High purity aluminum foils 17 μm thick were pressed on either side of the polymer to prevent material from flowing out of the spacer during heating. The sample assemblies were sealed in a hard X-ray-transparent aluminum-reinforced polypropylene pouch. SAXS measurements, described in ref 16, were performed at Beamline 7.3.3 at the Advanced Light Source synchrotron in Berkeley, CA.[38] The sample−detector distance was approximately 1.8 m and was calibrated using a silver behenate standard. A Pilatus 1M detector with a pixel size of 0.172 mm × 0.172

Table 1. Thermal History Profiles during the Thermal Annealing

temp (°C)	30	50	60	70	80	90	100	110	120	100	90	60	30
time (min)	30	40	100	90	90	90	90	80	140	60	53	40	12

mm was used to collect two-dimensional scattering patterns. A home-built heat stage was used to control the temperature. The isotropic two-dimensional scattering patterns were azimuthally integrated to produce one-dimensional scattering profiles using the Nika package for IgorPro.[39]

DPLS Measurement. A custom-designed apparatus for the DPLS measurement was used;[25] a schematic of the apparatus is shown in Figure 1. The light source used was a Coherent continuous wave (cw) diode laser with a fixed wavelength of 640 nm and an adjustable output from 0 to 40 mW. We selected 5 mW as the output power to avoid saturating the Lumenera CCD camera. As shown in Figure 1, the incident beam was redirected by a glass prism into a half-wave plate followed by a polarizer and an analyzer, with the heating block sandwiched in between. The half-wave plate was rotated to maximize the intensity of the incident beam transmitted through the polarizer.

A heating block surrounding the sample holder was used to control the sample temperature, using two heating elements and a channel for water circulation within the block. The heating elements were connected to an Omega Engineering temperature controller (CN9111A). Fast minimization of the difference between the process temperature and the set temperature was achieved by circulating water at the set temperature through the channel. The light transmitted through the analyzer, whose transmission axis was rotated 90° relative to the transmission axis of the polarizer, was reflected by a mirror and then projected onto an Edmundoptics ground glass screen. The Lumenera CCD camera, controlled by a custom-programmed interface, was used to record the scattering patterns incident on the screen. The scattering patterns were stored in the form of 8-bit, 480 × 640 pixel TIFF image files.

The DPLS sample was subjected to multistep quiescent isothermal annealing to quantitatively reproduce the thermal history of the isothermal annealing used in the SAXS measurements in ref 16. The DPLS sample was first heated from 30 to 120 °C and then cooled back to 30 °C; for each step during this heating–cooling process, the system was maintained at a constant temperature for a specific period of time as shown in Table 1. With the assistance of a Fisher-Scientific water bath, the sample temperature reached the set point in approximately 2–4 min for each step in both the heating and cooling process. A calibration was performed to relate the actual sample temperature to the set-point temperature on the controller and the water bath. The heating block was preheated to 30 °C, and the temperature was held at 30 °C for 20 min before the sample was loaded into the heating block. The interface was activated to begin recording the scattering patterns immediately after the sample was loaded (the elapsed time, $t = 0$ min), and a scattering pattern was captured at the end of each temperature step.

In a separate experiment, two DPLS patterns were obtained from a freshly prepared sample at room temperature using two lasers with different wavelengths. First, a scattering pattern was recorded using the Coherent cw red diode laser (wavelength 640 nm), and then another pattern was recorded from the same sample with a Laserglow cw blue diode laser with a wavelength is 473 nm. The scattering patterns were saved for later analysis.

Polarized Optical Microscopy. POM has proven to be a useful tool in the characterization of grain growth and grain structure in BCP solutions,[20] and we have employed it here to help in the interpretation of our DPLS data. Unannealed samples were placed on the stage of a Nikon Eclipse E200 microscope. The light from the halogen illuminator was filtered using a Corning CS 4-65 green colored glass filter. Polarizing and analyzing filters were crossed at 90°. Images were recorded in the form of 1392 × 1040 pixel BMP files using a Lumenera INFINITY 2-1RC CCD camera with INFINITY CAPTURE software.

DPLS Data Reduction and Analysis. Because the sample exhibited no ODT, we assumed that the sample was always filled with ordered lamellae. We employed the random uniaxial ellipsoidal

grain model, using the equations and fitting procedures described in ref 18, to obtain the average length and width parameters of the ellipsoidal grains, w, l, the average grain volume, $V = lw^2$, and the grain aspect ratio, l/w. This model has been successfully used to characterize an SEO electrolyte mixture with accessible ODT and several neat block copolymers.[18,19,25,40,41] The intensity of the scattered light illuminating the ground glass screen can be described as a function of q and μ and consists of two terms as shown in eq 1

$$I(q, \mu) = I_0[C_0(q; l, w) + C_4(q; l, w) \cos 4\mu] \quad (1)$$

where $q = 4\pi\lambda^{-1} \sin(\theta/2)$, θ is the polar scattering angle, μ is the azimuthal scattering angle, λ is the wavelength of the incident and scattered light, and I_0 is the intensity in the forward direction.

The $C_0(q;l,w)$ component dictates the overall decay of the scattered intensity as a function of q, l, and w; the $C_4(q;l,w)$ component is a measure of the depth of the 4-fold modulation of the scattering pattern. Analytic expressions for these two components can be found in ref 30. For spherical grains, i.e., $l/w = 1$, the scattered light intensity is azimuthally symmetric and reduces to eq 2.

$$I(q) = I_0 \exp\left(-\frac{q^2 w^2}{4}\right) \quad (2)$$

In our analysis, we obtained the estimated values of l, w, and I_0 through the least-squares fitting of the two experimentally extracted cosine moments, $f_0(q)$ and $f_4(q)$, to C_0 and C_4 according to eqs 3 and 4.

$$f_0(q) = \int_0^{2\pi} I(q, \mu) \, d\mu = 2\pi I_0 C_0(q; l, w) \quad (3)$$

$$f_4(q) = \int_0^{2\pi} I(q, \mu) \cos 4\mu \, d\mu = \pi I_0 C_4(q; l, w) \quad (4)$$

$$I_0 = K\phi V \quad (5)$$

According to eq 5, for a completely ordered sample, I_0 depends only on the grain volume, $V = lw^2$, because the proportionality constant, K, is approximately independent of temperature,[25] and the volume fraction of ordered grains, ϕ, is unity at all times.

The grain number density, ρ, can be calculated from

$$\rho = \phi/V \quad (6)$$

■ RESULTS AND DISCUSSION

Comparison between DPLS and SAXS. Reference 16 reported SAXS measurements of grain size as a function of temperature for a sample undergoing the multistep isothermal quench whose temperature profile is shown in Table 1. The grain size, L, is defined as $L = $ fwhm^{-1}, where fwhm is the full width at half-maximum of the primary SAXS peak associated with the lamellar structure of the sample. As shown in Figure 2, SAXS shows grain growth during heating, and little change in grain size during the subsequent cooling. In addition, the average grain sizes, L, measured by SAXS range from 10 to 80 nm, several orders of magnitude smaller than those typically measured by DPLS.

The results of DPLS measurements on a duplicate sample that has undergone the same thermal history as the SAXS sample are shown in Figures 3–5. Figure 3 shows images of depolarized scattering patterns at three different times. Two obvious features of these images are the angular spread and overall intensity both increasing with time. While an increase in intensity with time is the normal behavior for the time
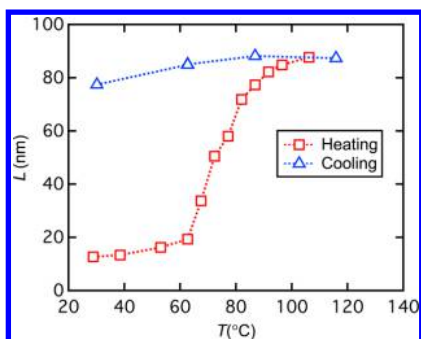
Figure 2. Dependence of grain size, L, on temperature, T, from SAXS data, based on ref 16.

Figure 4. Experimental development of spatially filtered intensity profiles, $I(q)$ vs q, along $\mu = 0°$ and $\mu = 45°$, at three times during the heating process.

evolution of block copolymer DPLS patterns as the volume fraction of grains increases, an increase in angular spread with time is a highly unusual feature and is an indicator of grains getting smaller with time. In all previous DPLS studies of grain evolution in block copolymers,[17−19,40,41] the angular spread decreased with time. Figure 4 displays plots of scattered intensity as a function of scattering vector for the patterns shown in Figure 3. The scattered intensity is nearly azimuthally symmetric, indicating that the ordered grains are nearly spherical on average (i.e., they are nearly rotationally symmetric in shape or there is no correlation between shape and optic axis).

After fitting the experimental scattering patterns to eqs 3 and 4, we obtain the grain parameters shown in Figure 5. In Figure 5a, one sees that I_0, the scattered DPLS intensity in the forward direction, obtained through a least-squares fit, increased by a factor of 2 as the temperature increased from 30 to 120 °C. Since K is roughly constant and $\phi = 1$ throughout the heating period, eq 8 suggests that the average grain volume doubled as the temperature increased from 30 to 120 °C. During the subsequent cooling process, little change in I_0 was observed. These results are qualitatively similar to the SAXS results; compare Figures 5a and Figure 2. In Figure 5, parts b and c, the average grain width, w, and the aspect ratio, l/w, are plotted as a function of temperature. The data points in Figure 5 represent the state of the grains during the last minute of the time period corresponding to that temperature. The width parameter, w, decreases from 12 to 8 μm as the temperature increases, while in the cooling period, w is independent of temperature. The aspect ratio was 1.75 ± 0.25 during the entire heating and
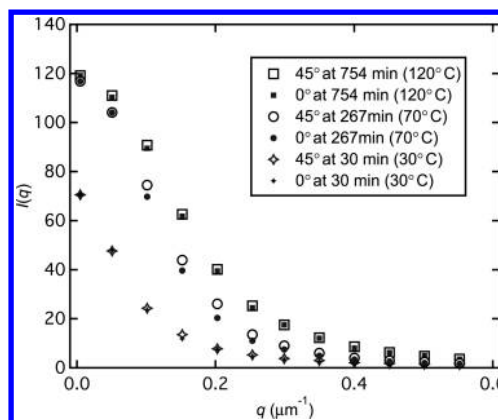
cooling process, consistent with the near azimuthal symmetry of the scattering patterns. While both DPLS and SAXS measurements show substantial grain size changes during heating and little change during cooling, the observed trends seem contradictory.

The grain evolution in a fully ordered sample with a decrease in the average grain dimensions is at odds with our current understanding of the kinetics of grain growth by defect annihilation.[16,17,42−45] In addition, in the same DPLS measurement, we obtain two apparently contradictory temperature dependences of the average grain size determined from the angular spread of the scattered intensity and from the absolute scattered intensity in forward direction. To understand these unusual features associated with DPLS measurements on an electrolyte mixture that cannot be disordered, we need to consider the specifics of the grain evolution in such samples, as well as the limitations of both the SAXS and DPLS techniques.

The grain evolution in an electrolyte mixture with no ODT starts with a set of pre-existing grains that is created during the sample preparation by freeze-drying. We posit that freeze-drying results in an extremely wide range of sizes. In contrast, the grain evolution in a block copolymer with an accessible ODT can start with a completely disordered state and proceeds by nucleation and growth, resulting in the sample with a narrow range of grain sizes.

The determination of grain size by SAXS is limited by the experimental resolution of the widths of the X-ray scattering
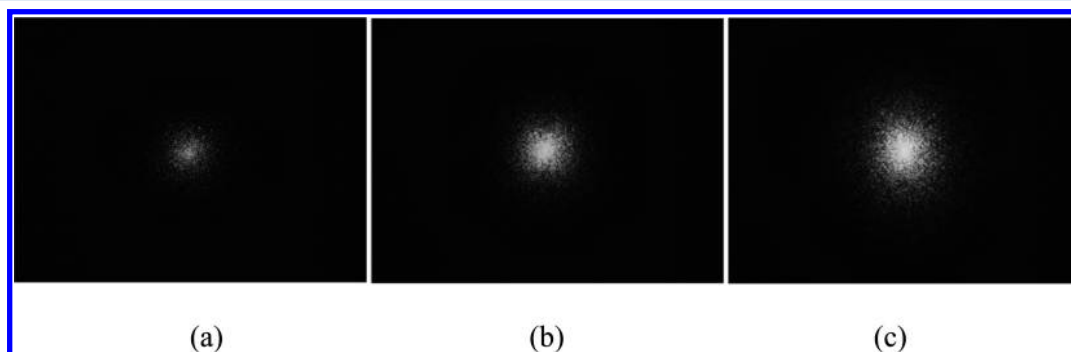

Figure 3. Parts a, b, and c represent depolarized scattering patterns captured at 30 min (30 °C), 267 min (70 °C), and 754 min (120 °C), respectively, with a sample heated from 30 to 120 °C. The maximum scattering vector q at the sides of each image is 1.13 μm^{-1}. The contrast of each pattern has been adjusted to enhance major features that are not clear in the original low-intensity patterns. Polarizer and analyzer are oriented vertically and horizontally in these images.
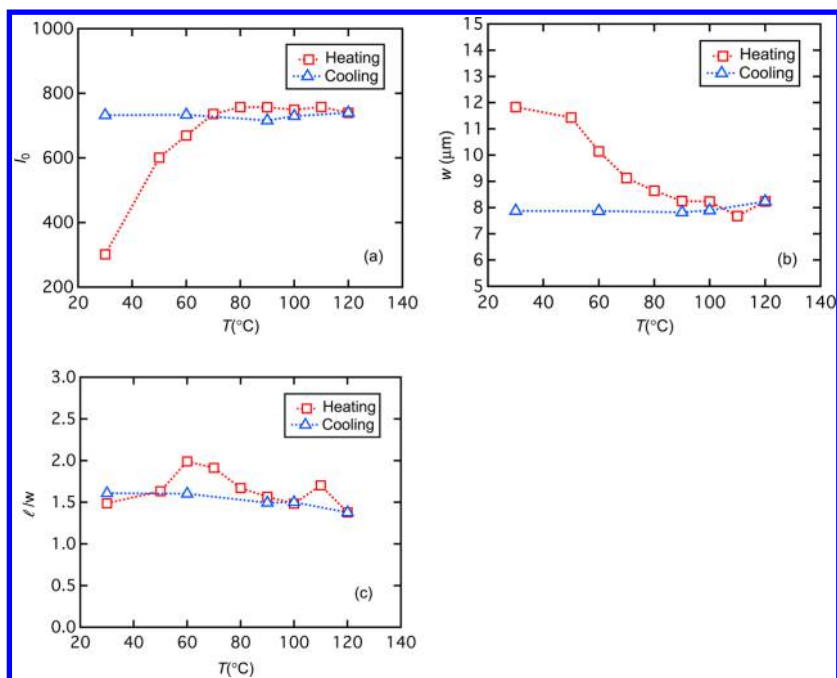
Figure 5. Temperature dependence of (a) the scattered intensity in the forward direction, I_0, (b) grain width parameter, w, and (c) grain aspect ratio, l/w, determined by DPLS.
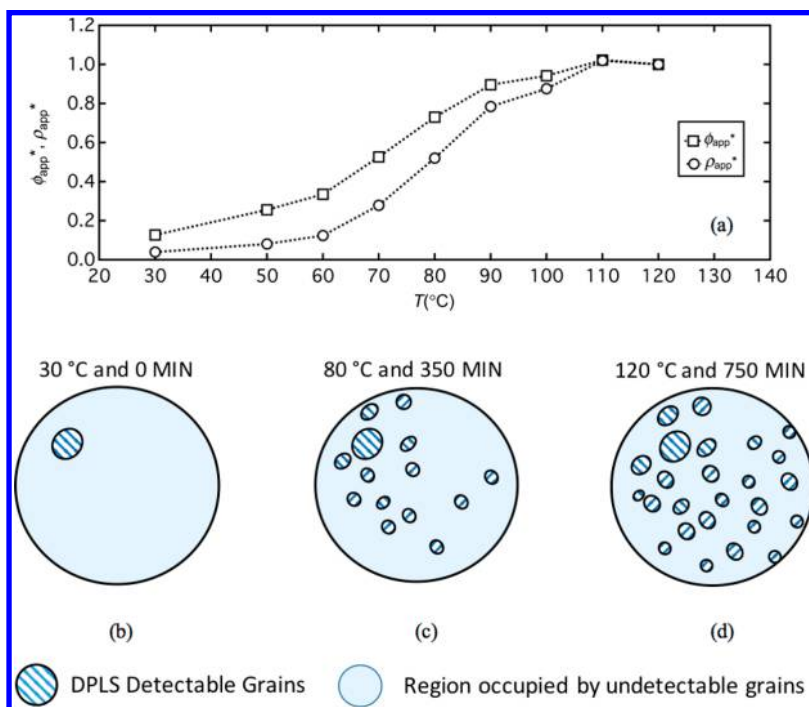

Figure 6. (a) Apparent grain volume fraction and apparent grain number density ϕ_{app}^* and ρ_{app}^* determined by DPLS are plotted versus temperature during the heating period. (b−d) Cartoons describing the detectable grain evolution during the heating period.

peaks. For the experimental conditions used to obtain Figure 2, the detector had a pixel size of 0.172 mm × 0.172 mm and was located approximately 1.8 m from the sample, and the X-ray source produced 10 keV monochromatic X-rays. This results in a q-resolution of 0.0125 nm^{-1}, which corresponds to a maximum detectable grain size of 80 nm. Thus, SAXS is only sensitive to the grains in the sample that are smaller than 80 nm.

Light scattering techniques such as DPLS are diffraction-limited methods that are intrinsically poor at detecting structures that are smaller than the wavelength of the light. The detection of very small grains is difficult because (1) the scattered intensity is proportional to the grain volume and (2) the angular spread of the scattered light is inversely related to the grain diameter. Thus, in a light scattering pattern from a sample consisting of a wide range of grain sizes, the smallest grains will contribute a negligible intensity to the pattern. For

example, a 10 μm grain contributes a million times the intensity as a 0.1 μm grain. Furthermore, assuming the incident light has a wavelength of 1 μm, the 10 μm grain scatters its light into a cone centered around the forward direction with an angle of ~2°, while the 0.1 μm grain scatters its light almost uniformly at all angles and thus contributes a negligible uniform background intensity to the scattering pattern.

If we imagine that the detectable DPLS scattering pattern arises from a subset of large grains in the completely ordered sample, then the remaining portion of the sample is effectively behaving optically as if it were disordered. The grain volume obtained by the analysis of the experimentally measured scattering pattern is then an "apparent" average volume, V_{app}, and the volume fraction of detectable grains becomes an apparent volume fraction, ϕ_{app}, of ordered grains. The increase in I_0 shown in Figure 3 is now interpreted not as an increase in average grain volume, but as an increase in ϕ_{app}. As small, undetectable grains grow larger, they eventually grow large enough to be detected and then add to the apparent ordered volume fraction.

As shown below, eqs 5 and 6 can be transformed into eqs 7 and 8 by replacing ϕ, V, and ρ with ϕ_{app}, V_{app}, and ρ_{app}, respectively, where ρ_{app} is apparent grain number density, which represents the number density of detectable grains within the illuminated volume.

$$I_0 = K\phi_{app}V_{app} \tag{7}$$

$$\rho_{app} = \frac{\phi_{app}}{V_{app}} \tag{8}$$

Assuming K is approximately independent of temperature, we define a relative volume fraction at temperature T, $\phi_{app}^* = \frac{K(T)\phi_{app}(T)}{K(120\ ^\circ C)\phi_{app}(120\ ^\circ C)} \simeq \frac{\phi_{app}(T)}{\phi_{app}(120\ ^\circ C)}$ to evaluate the change of the apparent volume fraction throughout the heating period, where $K(T)\phi(T)$ is calculated using eq 7. Both I_0 and V_{app} are obtained through least-squares fits to the experimental scattering patterns captured at the end of each quench step, in the same way as was done for the data in Figure 2. We also define a relative grain number density at temperature T, $\rho_{app}^* = \frac{K(T)\rho_{app}(T)}{K(120\ ^\circ C)\rho_{app}(120\ ^\circ C)} \simeq \frac{\rho_{app}(T)}{\rho_{app}(120\ ^\circ C)}$ to evaluate the change of the number density of detectable grains. In Figure 5a, we plot the ρ_{app}^* and ϕ_{app}^* versus quench temperatures.

We believe the apparent discrepancies between the results of DPLS and SAXS measurements come from the wide distribution of grain sizes of the pre-existing grains formed by freeze-drying from solution. Furthermore, both techniques are needed to detect the full range of this wide distribution. The grain evolution based on this view is shown in Figure 6b−d. According to Figure 6a, both the apparent grain number density and apparent volume fraction from DPLS are increasing with increasing temperature. In Figures 6b−d we show cartoons to describe how the apparent grain distribution is evolving with time. The grains that are detectable in the freshly prepared freeze-dried sample are depicted in Figure 6b. At later times, depicted in Figure 6c, in addition to the large grains that were present at the beginning, smaller grains have grown large enough to become detectable. With increasing time and annealing temperature, more small grains become detectable as shown in Figure 6d.

Bimodal Grain Distribution Model. In order to test our hypothesis concerning the limited detectability of small grains, we have attempted to develop as simple a grain distribution model as possible that exhibits the essential features of our DPLS data. We consider a block copolymer sample that is completely occupied by grains. For rotationally symmetric grains of width w, a correlation function analysis yields a depolarized scattered intensity, $I(q)$, incident on a detector plane perpendicular to the incident beam given by

$$I(q) = 0.003k^4\pi^{3/2}V_s w^3 I_i n^2(n_e - n_o)^2 \exp\left(-\left(\frac{qw}{2}\right)^2\right) \tag{9}$$

where k is the wavenumber of the light, V_s is the illuminated sample volume, I_i is the incident light intensity, n_e and n_0 are the extraordinary and ordinary refractive indices, n is the average refractive index, and q is the magnitude of the scattering vector.

For convenience, we re-express the scattered intensity in terms of the grain volume, $v = w^3$. We take eq 9 to represent the power contributed by grains whose volume is between v and $v + dv$. For this set of grains, V_s is replaced by $vN(v)\ dv$, where $N(v)\ dv$ is the number of grains in this interval. Then for a full distribution of grain sizes

$$I(q) = \kappa \int N(v, t)v^2 \exp\left(-\frac{q^2 v^{2/3}}{4}\right) dv \tag{10}$$

where κ is $0.003k^4\pi^{3/2}I_i n^2(n_e - n_o)^2$. As the grains in a sample evolve with time, they grow in size. Since the total sample volume is fixed, grains can only grow by merging with other grains. Thus, the time-dependent volume distribution $N(v,t)$ must satisfy the condition

$$\int_0^{v_{max}} N(v, t)v\ dv = V_{total} \tag{11}$$

where v_{max} is the volume of the largest grain and V_{total} is the total illuminated volume of the sample. The total number of grains at time t, $N_{total}(t)$, is given by

$$N_{total}(t) = \int_0^{v_{max}} N(v, t)\ dv \tag{12}$$

As grains grow, the total number of grains decreases, and their volumes increase with time. The expression for the total detectable scattered intensity is given by

$$I(q, t) = \kappa \int_{v_{th}}^{v_{max}} N(v, t)v^2 \exp\left(-\frac{q^2 v^{2/3}}{4}\right) dv \tag{13}$$

where v_{th} is the smallest grain volume that can be detected because of the limited collimating properties of the experimental apparatus. This threshold grain volume is related to a threshold grain width, w_{th}, by the relation $v_{th} = w_{th}^3$. The actual and apparent average grain volumes can be calculated from the time-dependent grain volume distribution from the equations

$$\langle v \rangle_{actual} = \frac{\int_0^{v_{max}} vN(v, t)\ dv}{\int_0^{v_{max}} N(v, t)\ dv} \tag{14}$$

$$\langle v \rangle_{\text{apparent}} = \frac{\int_{v_{\text{th}}}^{v_{\text{max}}} vN(v, t)\, dv}{\int_{v_{\text{th}}}^{v_{\text{max}}} N(v, t)\, dv} \tag{15}$$

In our model, the actual volume occupied by grains is unity throughout the time evolution, but we can calculate an apparent volume fraction of grains by summing over only those grains whose volumes are greater than the threshold volume.

$$\phi_{\text{app}} = \frac{\int_{v_{\text{th}}}^{v_{\text{max}}} vN(v, t)\, dv}{\int_{0}^{v_{\text{max}}} vN(v, t)\, dv} \tag{16}$$

A realistic grain volume distribution must be consistent with two characteristic features of the experimental DPLS data during the heating portion of the annealing process: (1) the apparent grain width decreases by a factor of 1.5 (Figure 5b), which corresponds to a decrease in the apparent grain volume by a factor of $1.5^3 \sim 3.3$, and (2) the apparent grain volume fraction increases by a factor of 7 (Figure 6a). The first condition places severe restrictions on the form of a suitable volume distribution. It rules out all single-peaked distributions, including normal (Gaussian) and log-normal distributions, which, according to eq 15, yield an apparent average grain volume that increases monotonically as the peak volume of the distribution increases. The simplest volume distribution that can exhibit a decrease in the apparent grain volume is a double-peaked distribution. We assume that the volume distribution consists of two parts, a and b. Part a describes a population of very small grains, while part b describes a population of large grains. If we allow the volumes in both populations to grow at the same rate (dv/dt), the fractional increase in the small grain volumes will be substantial, while the fractional increase in large grain volumes will be negligible. For simplicity, we assume that the large grain distribution (part b) is fixed over the time scale of our simulations. For the distribution parameters we have used, fixing the part b distribution changes the calculated quantities by less that 3%.

For ease of computation, we take each distribution to be "rectangular", having constant amplitudes $A_a(t)$ and A_b over a range of volumes (see Figure 7). We take the width of each
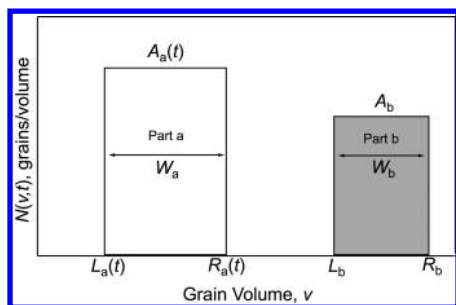

Figure 7. Bimodal population distribution at time t. Unshaded rectangle is part a, and shaded rectangle is part b.

distribution to be constants W_a and W_b, with left-hand and right-hand volume limits of $L_a(t)$ and $R_a(t) = L_a(t) + W_a$ for part a and L_b and $R_b = L_b + W_b$ for part b. (The actual grain distributions are likely to be much more complex; however, we show that many of our observations can be quantified by this simple model.) We allow $L_a(t)$ to increase linearly with time, which requires that the amplitude $A_a(t)$ decrease with time to

conserve sample volume, as shown in Figure 8. The second feature of the DPLS data, the increase in apparent volume
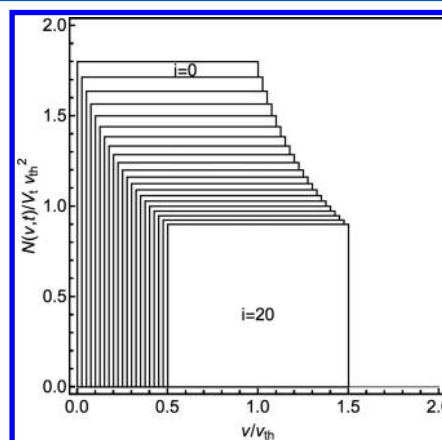

Figure 8. Time evolution of the small-grain portion (part a) of bimodal population distribution. The large-grain portion (part b) is off-scale and therefore not shown in this figure.

fraction with time, puts restrictions on the volume fractions of the a and b populations of grains. In particular, a large portion of the volume fraction must cross the threshold volume during the experiment. We assume that the initial small grain population ranges in size from zero to the threshold volume and that by the end of the experiment half of that population has exceeded the threshold. To ensure that the volume fraction that crosses the threshold is sufficiently large, we have chosen the small grain volume fraction to be $\phi_a = 0.9$ and the large grain volume fraction to be $\phi_b = 0.1$. We have also chosen the position of the fixed b distribution to produce the required 3-fold decrease in apparent average grain volume during the experiment. Using the moving small-grain distribution shown in Figure 8 and a fixed large-grain distribution given by $L_b = 5v_{\text{th}}$ and $R_b = 15v_{\text{th}}$, we have computed the resulting scattered intensity at discrete time intervals t_i, where $i = 0-20$, calculated from eq 13. At the start of the run ($i = 0$), $L_a(t_0) = 0$ and $R_a(t_0) = v_{\text{th}}$, so that all of the small grains are below the detection limit. At the end of the run ($i = 20$), $L_a(t_{20}) = 0.5v_{\text{th}}$ and $R_a(t_{20}) = 1.5v_{\text{th}}$, so that half of the small grains are detectable. All model plots employ dimensionless volumes, v/v_{th}, and dimensionless scattering vectors, $qv_{\text{th}}^{1/3}$.

For this bimodal grain distribution, the integrals in eq 10 can be evaluated analytically. The resulting $I(q,t)$ distributions are shown in Figure 9. They show the same trend as the experimental $I(q,t)$ distributions shown in Figure 4. To get a
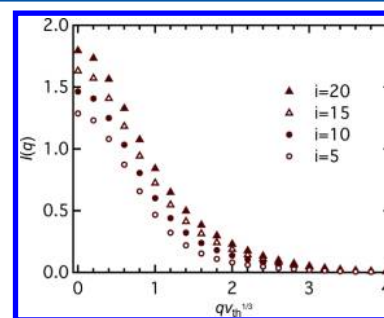

Figure 9. Calculated intensity $I(q)$ versus q for the bimodal population distribution at several different time steps.
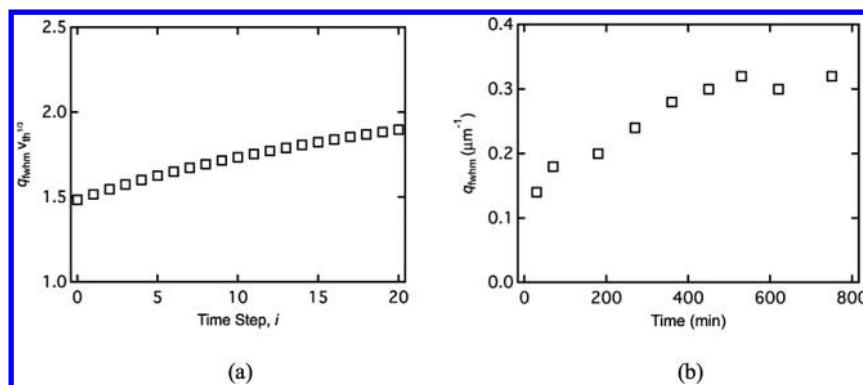
Figure 10. Full width at half-maximum of $I(q)$ vs q as a function of time based on (a) model calculations and (b) experiment.

better idea of the relative widths of these distributions, we also plot q_{fwhm}, the full width at half-maximum of the $I(q)$ vs q plot, as a function of time, in Figure 10a. The full width at half-maximum increases monotonically with time, as does the same plot based on the experimental data shown in Figure 10b. Since q_{fwhm} is inversely proportional to the average grain size, we conclude that the apparent grain size is decreasing with time, leveling off to a constant value.

Figure 11 shows the plots of these average grain volumes as a function of time. The actual average grain volume grows
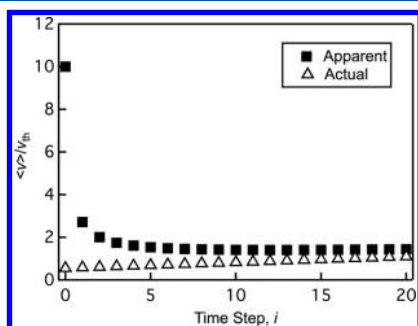

Figure 11. Actual and apparent average grain volume as a function of time from model calculation.

monotonically with time, while the apparent grain volume decreases sharply at early times, leveling off to a constant volume at long times. This is qualitatively similar to the changes in the experimentally observed average grain size shown in Figure 5b, although the decrease is steeper. This steep decrease seen in Figure 11 is probably an artifact of the "rectangular" small grain distribution; a Gaussian small grain distribution would have produced a more gradual decrease in the apparent average volume. Figure 11 shows a decrease in grain volume by a factor of 6.7, which corresponds to a change in grain width of $6.7^{1/3} = 1.9$, which is in reasonable agreement with the experimentally observed decrease in grain width by a factor of 1.5. Quantitative agreement between Figure 11 and Figure 5b would require that $10v_{th} = (12 \ \mu m)^3$ or $w_{th} = 5.6 \ \mu m$. This same value of w_{th} gives reasonable quantitative agreement between Figures 10a and 10b. Based on a light source with wavelength of 0.64 μm, such a threshold width seems too high. On the other hand, our model is almost certainly a great over-simplification of the grain distribution in the actual sample. The grains in our samples are probably highly irregular in shape and very narrow in certain dimensions, which would make them

below the threshold for detection even when their average widths are fairly large.

Figure 12 shows a plot of apparent volume fraction as a function of time. This plot shows the apparent volume fraction
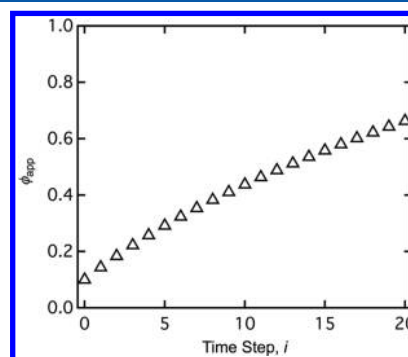

Figure 12. Apparent volume fraction vs time from model calculation.

increasing from about 0.1 to 0.66 over the course of the time evolution of the sample. Thus, the apparent volume fraction is increasing by a factor of 6.6, which is in good agreement with experimentally calculated relative apparent volume fraction shown in Figure 6, which increases by a factor of about 7.

POM Images of an Unannealed Sample. Figure 13 shows a POM image of an unannealed, completely ordered SEO/LiTFSI sample held between crossed polarizers. In this figure, one sees a dark background punctuated by small bright features, whose sizes range from about 5 to 50 μm. This image is reminiscent of the cartoons in Figure 6. We interpret the bright regions to be large birefringent grains and the dark background region to be filled with sub-micrometer grains that are not detectable by polarized optical microscopy. This interpretation is consistent with and corroborates the bimodal grain distribution picture that emerged from our analysis of the depolarized light scattering data.

DPLS Measurements with Two Wavelengths. DPLS scattering patterns were obtained from an unannealed sample at room temperature by using two lasers with wavelengths of 473 and 640 nm, under otherwise identical experimental conditions. As shown in Figure 14, the spread of the 473 nm pattern is significantly greater than that of the 640 nm pattern, and least-squares fitting yields an apparent grain width of 12 μm with 473 nm light and 23 μm with 640 nm light. The result is consistent with our hypothesis that fully ordered samples prepared by freeze-drying from solution contain a broad distribution of grain sizes, and that DPLS with a shorter wavelength of light is
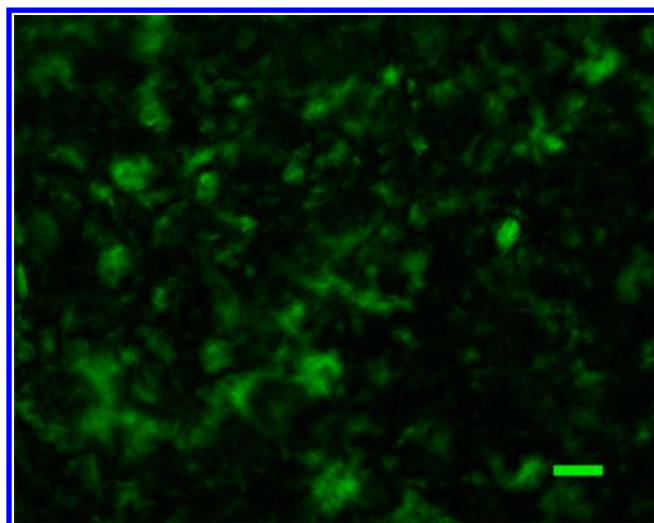
Figure 13. POM micrograph of an unannealed sample held between crossed polarizers and illuminated with green light at room temperature. The green scale bar in the lower right-hand corner is 50 μm long. The bright green features are large birefringent grains ranging in size from about 5 to 50 μm. The dark background is filled with sub-micrometer grains that are undetectable by both DPLS and POM.
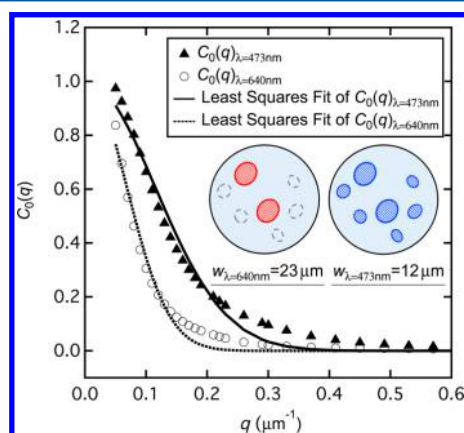

Figure 14. Least-squares fit of experimentally extracted, $C_0(q)$, from the scattering patterns captured from an unannealed sample at room temperature, using lasers with wavelengths of 473 and 640 nm.

capable of detecting smaller grains than DPLS with a longer wavelength. This is shown schematically in the inset to Figure 14, in which the blue laser is capable of detecting a population of small grains that is undetectable with the red laser.

■ CONCLUSIONS

In summary, although DPLS and SAXS have proven to be effective techniques for independently elucidating the grain structure of ordered block copolymer materials, there are BCP samples for which a combination of DPLS and SAXS is needed to provide a complete picture of the grain structure. This is especially true for samples in which there is a wide range of grain sizes and a significant population of grains that are smaller than the wavelength of the incident light used in DPLS. While we have shown that such distributions arise naturally in BCP samples prepared by freeze-drying from solution, other processing methods may result in wide distributions. For such samples, DPLS overestimates the average grain size and

underestimates the grain volume fraction because the small, subwavelength grains are not detectable, while SAXS underestimates the average grain size because it is insensitive to grains larger than 0.1 μm. Our results suggest that only grains with sizes larger than about 5 μm can be detected by DPLS using 640 nm light. Additional DPLS measurements with 473 nm light enable detection of smaller grains. A simple bimodal population model was used to interpret the DPLS data. This model was confirmed by the analysis of POM images. The present work is only the first step toward characterization of block copolymer samples with wide grain size distributions.

■ AUTHOR INFORMATION

Corresponding Author
*(B.A.G.) E-mail: bgaretz@nyu.edu.
Notes
The authors declare no competing financial interest.

■ ACKNOWLEDGMENTS

■ ABBREVIATIONS

BCP	block copolymer
BMP	bitmap image file
CCD	charge coupled device
DPLS	depolarized light scattering
fwhm	full width at half-maximum
TIFF	tagged image file format
LiTFSI	lithium bis(trifluoromethanesulfonyl)imide
ODT	order−disorder transition
PDI	polydispersity index
PEO	poly(ethylene oxide)
POM	polarized optical microscopy
PS	polystyrene
SAXS	small-angle X-ray scattering
SEO	polystyrene-b-poly(ethylene oxide) diblock copolymer

Symbols

$A_a(t)$	evolving amplitude of part a in bimodal distribution, grains/grain volume
A_b	fixed amplitude of part b in bimodal distribution, grains/grain volume
$C_0(q;l,w)$	azimuthally symmetric component of theoretical scattered intensity, dimensionless
$C_4(q;l,w)$	4-fold modulated component of theoretical scattered intensity, dimensionless
$f_0(q)$	zeroth cosine moment of experimental scattered intensity, dimensionless
$f_4(q)$	fourth cosine moment of experimental scattered intensity, dimensionless
i	time step, dimensionless
$I(q,\mu)$	experimental scattered intensity as a function of q and μ, dimensionless[25]
$I(q,t)$	theoretical total detectable scattered intensity at time, t, dimensionless
I_0	experimental scattered intensity in forward direction, $q = 0$, dimensionless
I_i	intensity of the incident light, dimensionless

K	proportionality constant, as a function of temperature, μm^{-3}	
k	wavenumber of incident light, μm^{-1}	
l	average grain length, μm	
l/w	average aspect ratio, dimensionless	
L	average grain dimension by SAXS, nm	
$L_a(t)$	evolving lower bound of the volume distribution of part a, μm	
L_b	lower bound of the volume distribution of part b, μm	
$N(v,t)$	number of grains with grain volume, v, per unit volume at time t, μm^{-3}	
$N(v)$	number of grains with grain volume, v, per unit volume, μm^{-3}	
$N_{total}(t)$	total number of grains at time, t, dimensionless	
n	average refractive index of a grain, dimensionless	
n_e	extraordinary refractive index of a grain, dimensionless	
n_o	ordinary refractive index of a grain, dimensionless	
q	magnitude of scattering vector, μm^{-1}	
q^*	the position of primary peak of SAXS intensity profile, nm^{-1}	
q_{fwhm}	full width at half-maximum in $I(q)$ vs q plot, μm^{-1}	
r	lithium salt concentration, dimensionless	
$R_a(t)$	evolving upper bound of the volume distribution of part a, μm	
R_b	upper bound of the volume distribution of part b, μm	
t	elapsed time, minute	
T_{ODT}	order-to-disorder transition temperature, °C	
T	sample temperature, °C	
V	average grain volume, μm^3	
V_{app}	apparent average grain volume by DPLS, μm^3	
V_s	illuminated sample volume, μm^3	
V_{total}	total illuminated sample volume, μm^3	
v	the volume of an individual grain, μm^3	
v_{max}	the volume of the largest grain, μm^3	
v_{th}	the smallest grain volume that can be detected because of the limited collimating properties of the experimental apparatus, μm^3	
$\langle v \rangle_{actual}$	the actual average grain volume, μm^3	
$\langle v \rangle_{apparent}$	the apparent average grain volume, μm^3	
w	average grain width, μm	
$w_{\lambda=640\ nm}$	the apparent average grain width determined by DPLS with $\lambda = 640$ nm, μm	
$w_{\lambda=473\ nm}$	the apparent average grain width determined by DPLS with $\lambda = 473$ nm, μm	
W_a	the width of the rectangular distribution of part a, μm	
W_b	the width of the rectangular distribution of part b, μm	

Greek Letters

ϕ	grain volume fraction, dimensionless	
ϕ_{app}	the apparent volume fraction of the ordered grains, dimensionless	
ϕ_{app}^*	the relative volume fraction of ordered grains, dimensionless	
λ	wavelength of incident light, nm	
θ	polar scattering angle, rad	
μ	azimuthal scattering angle, rad	
ρ	grain number density, number of grains per unit volume, μm^{-3}	
ρ_{app}	the apparent grain number density, μm^{-3}	
ρ_{app}^*	the relative grain number density, dimensionless	

κ $\quad$ $0.003 k^4 \pi^{3/2} I_i n^2 (n_e - n_o)^2$

■ REFERENCES

(1) Quartarone, E.; Mustarelli, P. Electrolytes for solid-state lithium rechargeable batteries: recent advances and perspectives. *Chem. Soc. Rev.* **2011**, *40* (5), 2525−2540.

(2) Young, W. S.; Kuan, W. F.; Epps, T. H. Block Copolymer Electrolytes for Rechargeable Lithium Batteries. *J. Polym. Sci., Part B: Polym. Phys.* **2014**, *52* (1), 1−16.

(3) Stone, G. M.; Mullin, S. A.; Teran, A. A.; Hallinan, D. T.; Minor, A. M.; Hexemer, A.; Balsara, N. P. Resolution of the Modulus versus Adhesion Dilemma in Solid Polymer Electrolytes for Rechargeable Lithium Metal Batteries. *J. Electrochem. Soc.* **2012**, *159* (3), A222−A227.

(4) Gu, Y. Y.; Zhang, S. P.; Martinetti, L.; Lee, K. H.; McIntosh, L. D.; Frisbie, C. D.; Lodge, T. P. High Toughness, High Conductivity Ion Gels by Sequential Triblock Copolymer Self-Assembly and Chemical Cross-Linking. *J. Am. Chem. Soc.* **2013**, *135* (26), 9652−9655.

(5) Zhang, H.; Liu, C. Y.; Zheng, L. P.; Xu, F.; Feng, W. F.; Li, H.; Huang, X. J.; Armand, M.; Nie, J.; Zhou, Z. B. Lithium bis(fluorosulfonyl)imide/poly(ethylene oxide) polymer electrolyte. *Electrochim. Acta* **2014**, *133*, 529−538.

(6) Marcinek, M.; Syzdek, J.; Marczewski, M.; Piszcz, M.; Niedzicki, L.; Kalita, M.; Plewa-Marczewska, A.; Bitner, A.; Wieczorek, P.; Trzeciak, T.; Kasprzyk, M.; Lezak, P.; Zukowska, Z.; Zalewska, A.; Wieczorek, W. Electrolytes for Li-ion transport - Review (vol 276, pg 107, 2015). *Solid State Ionics* **2015**, *282*, 95−95.

(7) Zhang, L.; Chaloux, B. L.; Saito, T.; Hickner, M. A.; Lutkenhaus, J. L. Ion Conduction in Poly(ethylene oxide) Ionically Assembled Complexes. *Macromolecules* **2011**, *44* (24), 9723−9730.

(8) Bates, C. M.; Chang, A. B.; Schulze, M. W.; Momcilovic, N.; Jones, S. C.; Grubbs, R. H. Brush Polymer Ion Gels. *J. Polym. Sci., Part B: Polym. Phys.* **2016**, *54* (2), 292−300.

(9) Diederichsen, K. M.; Brow, R. R.; Stoykovich, M. P. Percolating Transport and the Conductive Scaling Relationship in Lamellar Block Copolymers under Confinement. *ACS Nano* **2015**, *9* (3), 2465−2476.

(10) Leibler, L. Theory of Microphase Separation in Block Co-Polymers. *Macromolecules* **1980**, *13* (6), 1602−1617.

(11) Fredrickson, G. H.; Helfand, E. Fluctuation Effects in the Theory of Microphase Separation in Block Copolymers. *J. Chem. Phys.* **1987**, *87* (1), 697−705.

(12) Bates, F. S. Polymer-Polymer Phase-Behavior. *Science* **1991**, *251* (4996), 898−905.

(13) Lin, C. C.; Jonnalagadda, S. V.; Kesani, P. K.; Dai, H. J.; Balsara, N. P. Effect of Molecular-Structure on the Thermodynamics of Block-Copolymer Melts. *Macromolecules* **1994**, *27* (26), 7769−7780.

(14) Balsara, N. P.; Marques, C. M.; Garetz, B. A.; Newstein, M. C.; Gido, S. P. Anisotropy of lamellar block copolymer grains. *Phys. Rev. E: Stat. Phys., Plasmas, Fluids, Relat. Interdiscip. Top.* **2002**, *66*, 5.

(15) Majewski, P. W.; Yager, K. G. Reordering transitions during annealing of block copolymer cylinder phases. *Soft Matter* **2016**, *12* (1), 281−294.

(16) Chintapalli, M.; Chen, X. C.; Thelen, J. L.; Teran, A. A.; Wang, X.; Garetz, B. A.; Balsara, N. P. Effect of Grain Size on the Ionic Conductivity of a Block Copolymer Electrolyte. *Macromolecules* **2014**, *47* (15), 5424−5431.

(17) Dai, H. J.; Balsara, N. P.; Garetz, B. A.; Newstein, M. C. Grain growth and defect annihilation in block copolymers. *Phys. Rev. Lett.* **1996**, *77* (17), 3677−3680.

(18) Newstein, M. C.; Garetz, B. A.; Balsara, N. P.; Chang, M. Y.; Dai, H. J. Growth of grains and correlated grain clusters in a block copolymer melt. *Macromolecules* **1998**, *31* (1), 64−76.

(19) Kim, W. G.; Garetz, B. A.; Newstein, M. C.; Balsara, N. P. Maximizing the grain growth rate during the disorder-to-order transition in block copolymer melts. *J. Polym. Sci., Part B: Polym. Phys.* **2001**, *39* (19), 2231−2242.

(20) Chastek, T. Q.; Lodge, T. P. Grain shapes and growth kinetics during self-assembly of block copolymers. *J. Polym. Sci., Part B: Polym. Phys.* **2006**, *44* (3), 481−491.

(21) Lo, T. Y.; Ho, R. M.; Georgopanos, P.; Avgeropoulos, A.; Hashimoto, T. Direct Visualization of Order-Order Transitions in Silicon-Containing Block Copolymers by Electron Tomography. *ACS Macro Lett.* **2013**, *2* (3), 190−194.

(22) Hashimoto, T.; Sakamoto, N.; Koga, T. Nucleation and growth of anisotropic grain in block copolymers near order-disorder transition. *Phys. Rev. E: Stat. Phys., Plasmas, Fluids, Relat. Interdiscip. Top.* **1996**, *54* (5), 5832−5835.

(23) Floudas, G.; Pakula, T.; Fischer, E. W.; Hadjichristidis, N.; Pispas, S. Ordering Kinetics in a Symmetrical Diblock Copolymer. *Acta Polym.* **1994**, *45* (3), 176−181.

(24) Ryu, H. J.; Fortner, D. B.; Lee, S.; Ferebee, R.; De Graef, M.; Misichronis, K.; Avgeropoulos, A.; Bockstaller, M. R. Role of Grain Boundary Defects During Grain Coarsening of Lamellar Block Copolymers. *Macromolecules* **2013**, *46* (1), 204−215.

(25) Wang, X.; Thelen, J. L.; Teran, A. A.; Chintapalli, M.; Nakamura, I.; Wang, Z. G.; Newstein, M. C.; Balsara, N. P.; Garetz, B. A. Evolution of Grain Structure during Disorder-to-Order Transitions in a Block Copolymer/Salt Mixture Studied by Depolarized Light Scattering. *Macromolecules* **2014**, *47* (16), 5784−5792.

(26) Gunkel, I.; Thurn-Albrecht, T. Thermodynamic and Structural Changes in Ion-Containing Symmetric Diblock Copolymers: A Small-Angle X-ray Scattering Study. *Macromolecules* **2012**, *45* (1), 283−291.

(27) Zhu, L.; Cheng, S. Z. D.; Calhoun, B. H.; Ge, Q.; Quirk, R. P.; Thomas, E. L.; Hsiao, B. S.; Yeh, F.; Lotz, B. Phase structures and morphologies determined by self-organization, vitrification, and crystallization: confined crystallization in an ordered lamellar phase of PEO-b-PS diblock copolymer. *Polymer* **2001**, *42* (13), 5829−5839.

(28) Myers, R. T.; Cohen, R. E.; Bellare, A. Use of ultra-small-angle X-ray scattering to measure grain size of lamellar styrene-butadiene block copolymers. *Macromolecules* **1999**, *32* (8), 2706−2711.

(29) Hashimoto, T.; Nagatoshi, K.; Todo, A.; Hasegawa, H.; Kawai, H. Domain-Boundary Structure of Styrene-Isoprene Block Copolymer Films Cast from Toluene Solutions. *Macromolecules* **1974**, *7* (3), 364−373.

(30) Holzwarth, U.; Gibson, N. The Scherrer equation versus the 'Debye-Scherrer equation'. *Nat. Nanotechnol.* **2011**, *6* (9), 534−534.

(31) Scherrer, P. Estimation of the Size and Structure of Colloidal Particles by Rontgen Rays. Nachrichten von der K. Gesellschaft der. Wissenschaften zu Gottingen. *Math. Phys. Klasse* **1918**, *No. i*, 322−323.

(32) Teran, A. A.; Balsara, N. P. Thermodynamics of Block Copolymers with and without Salt. *J. Phys. Chem. B* **2014**, *118* (1), 4−17.

(33) Hadjichristidis, N.; Iatrou, H.; Pispas, S.; Pitsikalis, M. Anionic polymerization: High vacuum techniques. *J. Polym. Sci., Part A: Polym. Chem.* **2000**, *38* (18), 3211−3234.

(34) Quirk, R. P.; Kim, J.; Kausch, C.; Chun, M. S. Butyllithium-initiated anionic synthesis of well-defined poly(styrene-*block*-ethylene oxide) block copolymers with potassium salt additives. *Polym. Int.* **1996**, *39* (1), 3−10.

(35) Lascaud, S.; Perrier, M.; Vallee, A.; Besner, S.; Prud'homme, J.; Armand, M. Phase-Diagrams and Conductivity Behavior of Poly-(Ethylene Oxide) Molten-Salt Rubbery Electrolytes. *Macromolecules* **1994**, *27* (25), 7469−7477.

(36) Yuan, R.; Teran, A. A.; Gurevitch, I.; Mullin, S. A.; Wanakule, N. S.; Balsara, N. P. Ionic Conductivity of Low Molecular Weight Block Copolymer Electrolytes. *Macromolecules* **2013**, *46* (3), 914−921.

(37) Teran, A. A.; Mullin, S. A.; Hallinan, D. T.; Balsara, N. P. Discontinuous Changes in Ionic Conductivity of a Block Copolymer Electrolyte through an Order-Disorder Transition. *ACS Macro Lett.* **2012**, *1* (2), 305−309.

(38) Hexemer, A.; Bras, W.; Glossinger, J.; Schaible, E.; Gann, E.; Kirian, R.; MacDowell, A.; Church, M.; Rude, B.; Padmore, H. A Saxs/Waxs/Gisaxs Beamline with Multilayer Monochromator. *J. Phys.: Conf. Ser.* **2010**, *247*, 012007.

(39) Ilavsky, J. Nika: software for two-dimensional data reduction. *J. Appl. Crystallogr.* **2012**, *45*, 324−328.

(40) Kim, W. G.; Chang, M. Y.; Garetz, B. A.; Newstein, M. C.; Balsara, N. P.; Lee, J. H.; Hahn, H.; Patel, S. S. Effect of quench depth on grain structure in quiescently ordered block copolymers. *J. Chem. Phys.* **2001**, *114* (22), 10196−10211.

(41) Chang, M. Y.; Abuzaina, F. M.; Kim, W. G.; Gupton, J. P.; Garetz, B. A.; Newstein, M. C.; Balsara, N. P.; Yang, L.; Gido, S. P.; Cohen, R. E.; Boontongkong, Y.; Bellare, A. Analysis of grain structure in partially ordered block copolymers by depolarized light scattering and transmission electron microscopy. *Macromolecules* **2002**, *35* (11), 4437−4447.

(42) Chastek, T. Q.; Lodge, T. P. Twinning and growth kinetics of lamellar grains in a diblock copolymer solution. *J. Polym. Sci., Part B: Polym. Phys.* **2005**, *43* (4), 405−412.

(43) Bockstaller, M. R.; Ryu, H. J. On the relevance of defects on grain coarsening in block copolymer melts. *Abstr. Pap. Am. Chem. Soc.* **2012**, 244.

(44) Ryu, H. J.; Sun, J.; Avgeropoulos, A.; Bockstaller, M. R. Retardation of Grain Growth and Grain Boundary Pinning in Athermal Block Copolymer Blend Systems. *Macromolecules* **2014**, *47* (4), 1419−1427.

(45) Ryu, H. J.; Fortner, D. B.; Rohrer, G. S.; Bockstaller, M. R. Measuring Relative Grain-Boundary Energies in Block-Copolymer Microstructures. *Phys. Rev. Lett.* **2012**, *108*, 10.